

# Thermodynamic Descriptors from Molecular Dynamics as Machine Learning Features for Extrapolable Property Prediction

Nuria H. Espejo<sup>†,1,2</sup> Pablo Llombart<sup>†,1</sup> Andrés González de Castilla,<sup>3</sup> Jorge Ramirez,<sup>4,a)</sup> Jorge R. Espinosa,<sup>1,5,b)</sup> and Adiran Garaizar<sup>2,c)</sup>

<sup>1)</sup> *Department of Physical-Chemistry, Universidad Complutense de Madrid, Av. Complutense s/n, Madrid 28040, Spain*

<sup>2)</sup> *Data Science, Bayer AG, Alfred-Nobel-Straße 50, 40789 Monheim am Rhein, Germany*

<sup>3)</sup> *Crop Protection Innovation, Bayer AG, Kaiser-Wilhelm-Alle 1, 51373 Leverkusen, Germany*

<sup>4)</sup> *Department of Chemical Engineering, Universidad Politécnica de Madrid, C/ Jose Gutierrez Abascal 2, Madrid 28006, Spain*

<sup>5)</sup> *Yusuf Hamied Department of Chemistry, University of Cambridge, Lensfield Road, Cambridge CB2 1EW, UK*

<sup>†</sup> *These authors contributed equally to this work.*

(Dated: 13 March 2026)

Machine learning (ML) models which rely on molecular structure excel at predicting properties for well-represented organic compounds, however their limited ability to extrapolate to chemotypes outside their training domain, remains a critical bottleneck in chemical discovery. This challenge is particularly acute in industrial discovery, where navigating uncharted chemical space to generate new intellectual property is a primary objective. Normal boiling points serve as a key benchmark for testing the extrapolative power of ML algorithms. A major limitation is that group-contribution methods are by design unable to generate predictions for molecules containing unparameterized fragments. Here, we demonstrate that this limitation can be overcome by replacing structural descriptors with thermodynamic properties computed directly from molecular dynamics simulations. We introduce a physics-augmented framework where a CatBoost regression model learns directly from ensemble-averaged cohesive energies, heats of vaporization, and densities extracted from atomistic liquid-phase simulations. Benchmark comparisons reveal that while both our physics-augmented model and conventional structure-based models perform comparably well on standard organic compounds, only the former maintains controlled error growth when extrapolating to structurally dissimilar chemical space. Our model successfully predicts boiling points for chemical classes entirely absent from training—including inorganic compounds, salts, and molecules with elements like Si, B, and Te—where structure-based models are fundamentally inapplicable. By encoding the intermolecular forces governing phase behavior, our framework establishes a generalizable strategy for property prediction beyond the structural boundaries of the existing methods.

Keywords: Boiling points, Physics-Augmented Machine Learning, All-Atom Molecular Dynamics, Thermodynamic descriptors, Ionic liquids

## I. INTRODUCTION

The accurate prediction of macroscopic material properties from molecular structure is a foundational goal of computational chemistry, underpinning fields from drug discovery to materials science<sup>1,2</sup>. The utility, safety, and commercial viability of new compounds are dictated by a suite of physicochemical properties, including its solubility, viscosity, and phase behavior<sup>3,4</sup>. Among this diverse landscape of properties, those governing phase transitions are particularly fundamental. The normal boiling point (nBP), for instance, serves as a key benchmark for testing the generalization of any predictive framework<sup>5</sup>. This property is of immense practical impor-

tance, with broad relevance in pharmaceutical manufacturing, chemical engineering, sustainability, and safety assessment<sup>6-9</sup>. However, experimental determination, while well-established for many common substances, can be a low-throughput endeavor, with methodologies and costs that vary significantly based on the substance in question<sup>9-12</sup>. This challenge is particularly pronounced for difficult-to-measure or model compounds, such as active pharmaceutical ingredients (APIs)<sup>13</sup>, difficult-to-isolate systems including impurities<sup>14,15</sup>, salts and ionic liquids<sup>16</sup>. This gap between the industrial demand for reliable data and the limitations of current predictive tools has been identified as a key challenge for the future of applied thermodynamics, underscoring the urgent need for more robust and transferable models capable of navigating the novel chemical spaces essential for industrial innovation and intellectual property.<sup>17</sup>

A rich spectrum of methods has been developed to address nBP and vapor-pressure prediction. Classical

<sup>a)</sup> Electronic mail: [jorge.ramirez@upm.es](mailto:jorge.ramirez@upm.es)

<sup>b)</sup> Electronic mail: [jorgerene@ucm.es](mailto:jorgerene@ucm.es)

<sup>c)</sup> Electronic mail: [adiran.garaizar@bayer.com](mailto:adiran.garaizar@bayer.com)

approaches, such as corresponding-states methods<sup>18,19</sup>, exploit reduced-property correlations based on critical data, but their scope is limited when such data is unavailable, or the target molecule’s chemotype diverges significantly<sup>20</sup>. Group-contribution (GC) schemes<sup>21–30</sup>, like the well-known Joback<sup>31</sup> or Nannoolal<sup>32</sup> methods, decompose molecules into predefined structural fragments. While rapid, and highly effective for molecules that can be segmented into their parameterized groups, GC methods are structurally blind to compounds built from elements or motifs not encoded in their parameterized fragment libraries<sup>33</sup>. In a similar vein, equation-of-state (EoS) models like Peng–Robinson or SAFT<sup>34–36</sup> can offer physically motivated predictions, but only when reliable component-specific parameters are known or sufficient experimental data is available for their parameterization. At the other end of the spectrum are first-principles methods, with COSMO-RS being a prominent example<sup>37</sup>. This approach uses quantum mechanics to predict thermodynamic properties, such as vapor pressure, for a wide range of chemicals—including organics, mixtures and ionic liquids—without requiring compound-specific experimental data<sup>38–40</sup>. However, as a continuum-based model, COSMO-RS averages intermolecular interactions, which leads to documented quantitative failures and large deviations for systems governed by strong, specific forces, such as those in ionic liquids<sup>41,42</sup>.

The last two decades, however, have seen a revolution driven by the modern data-driven paradigm of Quantitative Structure-Property Relationship (QSPR) modeling<sup>43</sup>. This approach uses pre-calculated molecular descriptors to train a statistical model, from early efforts with multiple linear regression<sup>44–48</sup> to more advanced algorithms like Random Forest<sup>49</sup> or Gradient Boosting<sup>50</sup>. While powerful, the predictive capability of all these models is fundamentally limited by the expressiveness and transferability of manually engineered descriptors<sup>51</sup>.

A more recent breakthrough has been the evolution to deep learning, particularly Graph Neural Networks (GNNs), which they learn property-relevant representations directly from the molecular graph, bypassing the need for manual descriptor engineering<sup>52–54</sup>. This paradigm has been successfully applied to a wide array of thermophysical properties<sup>55–61</sup>, and it has become a dominant strategy for nBP prediction<sup>62–65</sup>. This approach has been notably successful, with state-of-the-art frameworks like GRAPPA<sup>66</sup>, achieving exceptional accuracy. Trained on tens of thousands of experimental data points, GNNs routinely outperform classical schemes within their training domain<sup>66</sup>. Indeed, recent work has shown that specialized GNNs can achieve high accuracy even for notoriously complex systems like ionic liquids, provided they are trained on vast, domain-specific datasets<sup>67</sup>. However, because they learn statistical associations from molecular topology without direct access to the thermodynamic state of the liquid, their performance is tightly coupled to the training data’s diversity<sup>68</sup>. When applied to molecules that are struc-

turally and physicochemically dissimilar from the training distribution, their extrapolative behavior becomes uncertain<sup>69</sup>. This effectively excludes many classes of novel, drug-like structures from their reliable applicability domain<sup>70,71</sup>. This limitation is particularly significant in industrial settings, where the primary goal is to generate intellectual property by exploring precisely these novel chemical domains.

The limitations of purely structural models motivate a direct solution: re-introducing the missing physics by using physics-based descriptors. This approach moves beyond the pre-defined structural descriptors—ranging from 2D fragments to 3D conformational properties—common in traditional QSPR, and instead computes features derived directly from first-principles simulations. One category of these descriptors is derived from quantum mechanics (QM), which provides a highly accurate description of a single molecule’s electronic structure<sup>72–74</sup>. However, while physically rigorous, these descriptors inherently describe a molecule in isolation, and thus neglect the crucial intermolecular interactions and ensemble effects that govern a condensed-phase property like the boiling point. A more direct approach is to use molecular dynamics (MD) simulations to explicitly model the molecular ensemble<sup>75–77</sup>. Indeed, computational studies have long leveraged MD to investigate phase transitions and related thermodynamic properties, from calculating vaporization enthalpies of complex fluids like ionic liquids<sup>78</sup> to characterizing liquid-vapor interfaces<sup>79</sup>, and determining phase equilibria from rigorous but computationally demanding free energy calculations<sup>80,81</sup>. However, these computational efforts have traditionally focused on either highly demanding, direct coexistence simulations to compute the nBP in the liquid-vapor equilibrium from scratch<sup>82</sup>, or on using simulation data to develop more accurate force fields<sup>83</sup>. The computational expense of such simulations, however, has remained a significant barrier to their routine use for generating descriptors at scale, creating a need for more efficient methodologies. The challenge, therefore, lies in creating a hybrid framework that harnesses the predictive efficiency of data-driven models while being firmly anchored in the physical principles that govern molecular behavior. This goal of anchoring data-driven models in physical principles is central to the emerging paradigm of Physics-Informed Machine Learning (PIML)<sup>84,85</sup>, has gained traction across diverse scientific domains<sup>86–91</sup>.

In this work, we implement a physics-augmented strategy specifically designed for scalable and extrapolative property prediction. We hypothesize that thermodynamic features derived from computationally tractable MD simulations can unlock robust generalization where purely structural models fail. We run short, all-atom simulations to compute descriptors such as the cohesive energy, and use these quantities as features to train a CatBoost<sup>92</sup> regression model. We show that this enables reliable extrapolation beyond the traditional domain of QSPR, successfully predicting boiling points for

chemical classes where structural models are often fragile or inapplicable, including inorganic compounds, complex charged systems like salts, and molecules containing uncommon elements such as tellurium and boron.

## II. MATERIALS AND METHODS

### A. Training and Test Sets

The initial training dataset was sourced from the curated compilation in Ref.<sup>49</sup>, which provides boiling point data for approximately 1,748 organic compounds (primarily hydrocarbons, alcohols, and amines) originally extracted from the CAS database<sup>93</sup>. To ensure the highest data quality, all experimental values were subsequently cross-verified against multiple authoritative databases: the NIST Chemistry WebBook<sup>94</sup>, PubChem<sup>11</sup>, and ChemSpider<sup>95</sup>. Compounds were excluded from our final dataset if they exhibited discrepancies greater than 10 K across sources, lacked corroborating entries, or were flagged with uncertainty markers. To ensure the physical validity of the simulations, a molecular weight threshold of 225 g/mol was applied. This step was necessary to exclude both low-molecular-weight compounds that would readily vaporize at the simulation temperatures (e.g., 300 K or 400 K) and high-molecular-weight compounds that would likely be solid or crystalline. In either case, the simulation would not represent a stable liquid-phase ensemble, invalidating the basis for our descriptor calculation. This filtering removed approximately 500 compounds, yielding a final training set of 1,280 entries with high-confidence experimental values. This collection forms the basis of our Training Set (available in section VI).

To rigorously evaluate model performance, two distinct test sets were curated, each designed to probe a different aspect of predictive capability. The first, a benchmark set for extrapolation, comprises active pharmaceutical ingredients (APIs) sourced from DrugBank<sup>96</sup>. These molecules were selected for their high structural complexity, often featuring more intricate scaffolds and a greater diversity of functional groups compared to the simpler, smaller molecules constituting the training set. These molecules, while structurally complex and diverse, are composed of standard organic elements. This composition ensures they fall within the theoretical applicability domain of modern cheminformatics-based predictors, enabling a direct, head-to-head comparison of our model’s extrapolative performance against state-of-the-art methods on challenging, real-world structures.

The second, an out-of-domain challenge set, was curated to rigorously test the model’s generalization capabilities on chemical classes that lie far outside the applicability domain of traditional QSPR. It comprises chemotypes—including ionic liquids, salts, and molecules containing non-standard elements such as B, Si, and Te—for which many standard models are fundamentally in-

applicable as they cannot generate a prediction for structures containing unparameterized elements or fragments. As a direct benchmark is therefore often impossible, predictions for this set are reported in order to characterize the model’s behavior and define the boundaries of its applicability in these challenging chemical spaces.

### B. Molecular Dynamics Simulations

To generate the thermodynamic descriptors for our model, we performed atomistic molecular dynamics (MD) simulations for all compounds. The following protocol constitutes the workflow necessary to generate features for each compound. To assess the robustness and transferability of the descriptors, we established two parallel and independent simulation workflows, each employing a different state-of-the-art force field.

The OpenFF workflow used the OpenFF-2.0.0 ‘Parsley’ force field<sup>97</sup>, with simulations run in the GROMACS 2025.2 package<sup>98</sup>. Separately, the OPLS4 workflow was run using the OPLS4 force field<sup>99</sup> as implemented in Schrödinger’s Materials Science Suite.

For each compound and for each of the two force fields, three independent NPT simulations of 20 ns were performed at 300, 400 and 500 K, all at 1 atm with a 2 fs integration time step. Simulation boxes contained approximately 15,000 atoms. Thermodynamic properties were averaged over the final 5 ns of each trajectory. From these trajectories, a set of thermodynamic descriptors was computed, including the cohesive energy ( $E_{\text{coh}}$ ), defined as the negative of the average intermolecular potential energy ( $E_{\text{coh}} = -\langle U_{\text{inter}} \rangle$ ), heat of vaporization ( $\Delta H_{\text{vap}} \approx E_{\text{coh}} + RT$ ), density ( $\rho$ ), the Hildebrand solubility parameter ( $\delta = \sqrt{(\Delta H_{\text{vap}} - RT)/V_m}$ ), and the isobaric specific heat capacity ( $C_P$ ). The latter was computed from enthalpy fluctuations via the relation  $C_P = (\langle H^2 \rangle - \langle H \rangle^2)/(k_B T^2)$ <sup>100</sup>.

#### 1. OpenFF Simulations

Molecular topologies were generated from SMILES strings using RDKit<sup>101</sup> and the OpenFF Toolkit, with Gasteiger<sup>102</sup> partial charges. Initial simulation boxes were built with Packmol<sup>103</sup>. Systems were then energy-minimized and equilibrated for 2 ns under NPT conditions in GROMACS 2025.2<sup>98</sup>.

Production runs were conducted using the leap-frog (md) integrator with a 2 fs time step. Long-range electrostatics were handled via the Particle Mesh Ewald (PME) method<sup>104</sup> with a short-range cutoff of 0.9 nm. Van der Waals interactions were treated with a cutoff at 0.9 nm, using a force-switching function that started at 0.8 nm to smoothly bring the forces to zero. Long-range dispersion corrections for energy and pressure were applied. The V-rescale thermostat<sup>105</sup> (1.0 ps relaxation

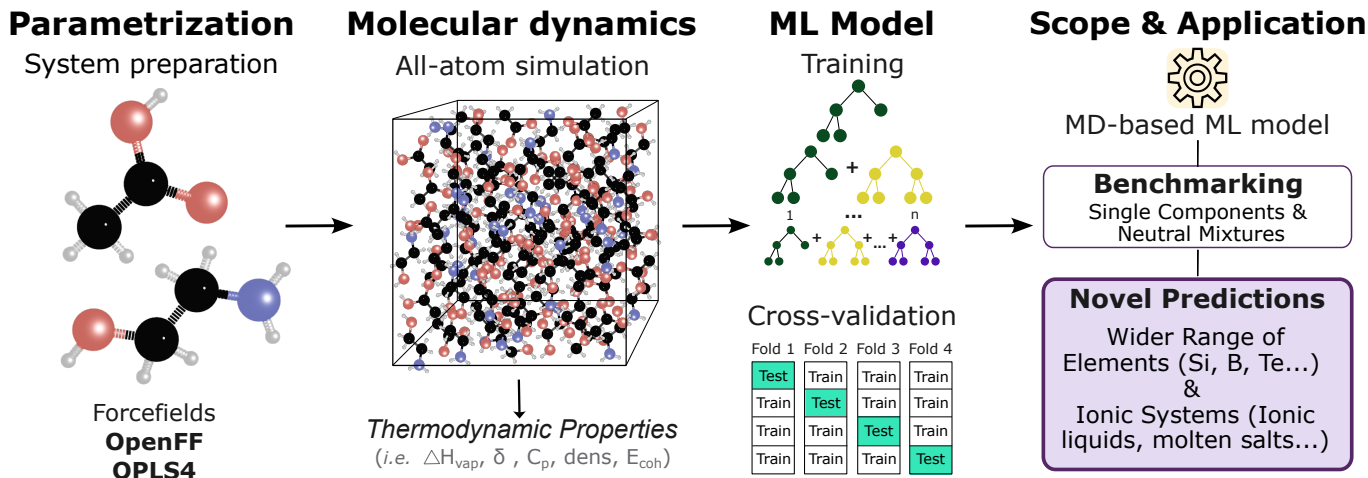


FIG. 1. Schematic of the physics-augmented workflow for normal boiling point prediction. Molecular structures are built from SMILES strings and subjected to short all-atom molecular dynamics simulations using the OPLS and OpenFF forcefields. Thermodynamics properties, including cohesive energy and heat of vaporization, are extracted from the simulations and used as physics-augmented descriptors to train a CatBoost regression model for the final boiling point prediction.

time, isotropic) and the C-rescale barostat (2.0 ps relaxation time) were used to maintain temperature and pressure, respectively. All bonds were constrained using the LINCS algorithm<sup>106</sup>.

To calculate  $E_{\text{coh}}$  in this workflow, the system was divided into two equal molecular subgroups. The total intermolecular potential energy between these subgroups (short-range Coulomb + van der Waals) was summed, and the resulting value,  $\langle U_{\text{inter}} \rangle$ , was inverted in sign and normalized by the number of molecules to yield the final cohesive energy.

## 2. OPLS4 Simulations

Systems were prepared using the Desmond System Builder in Maestro (Schrödinger Materials Science Suite). After energy minimization and multi-stage equilibration, production NPT runs of 20 ns were conducted using the Nosé–Hoover chain thermostat<sup>107</sup> (1 ps relaxation) and Martyna–Tobias–Klein barostat<sup>107</sup> (2 ps, isotropic). The RESPA integrator was employed with bonded/near/far time steps of 2.0/2.0/6.0 fs. Short-range Coulomb interactions were truncated at 0.9 nm. For this workflow, the cohesive energy ( $E_{\text{coh}}$ ) was computed as the negative of the average total intermolecular potential energy, extracted directly from Desmond’s simulation output.

## C. Machine Learning Model

The set of MD-derived descriptors was chosen based on a balance between their direct physical relevance to vaporization and their computational accessibility. Properties like cohesive energy and heat of vaporization directly quantify the intermolecular forces that must be

overcome during boiling. Density reflects the packing of molecules in the liquid phase, while the solubility parameter and the isobaric heat capacity provide composite measures of the system’s cohesive and thermal properties. Crucially, all these descriptors can be efficiently extracted from standard NPT simulations, providing a rich, physically-grounded feature set for the machine learning model without resorting to more computationally intensive protocols.

For each force field, three CatBoost<sup>92</sup> gradient-boosted regression models were trained:

- MD-only model:** Trained exclusively on MD-derived thermodynamic descriptors ( $E_{\text{coh}}$ ,  $\Delta H_{\text{vap}}$ ,  $\rho$ ,  $\delta$ ,  $C_p$ ) extracted at 300, 400 and 500 K.
- Chemoinformatics-only models:** Trained on a large set of chemoinformatics descriptors computed from SMILES strings using RDKit<sup>101</sup>. This feature set is composed of three main groups: (a) MACCS keys (166 bits), (b) Morgan circular fingerprints (radius 2, 2048 bits), and (c) a wide range of other 2D physicochemical descriptors, including properties like molecular weight, TPSA, hydrogen bond counts, and many others.
- Hybrid models:** Combined both MD-derived thermodynamic features and structural descriptors into a unified feature set.

Hyperparameter optimization was performed via Bayesian search using Optuna<sup>108</sup> with 50 trials. The training set (1280 compounds) was split using stratified 4-fold outer cross-validation scheme. The groups were generated by clustering the 1,280 training compounds based on structural similarity, using a sphere exclusion algorithm with Morgan fingerprints and a Tanimoto similarity threshold of 0.65. This procedure ensures that

structurally similar molecules are kept within the same fold, forcing the model to be validated on chemical scaffolds that are distinct from those seen during training in each split. For each outer fold, a 3-fold inner cross-validation loop was used for hyperparameter optimization, which was conducted via a 50-trial Bayesian search using Optuna<sup>108</sup>. Key optimized parameters included the learning rate, tree depth, L2 regularization, and the number of boosting iterations (up to 1000, with early stopping). Feature selection used CatBoost’s native importance scores. Our model performance was quantified using the mean absolute error (MAE), root mean squared error (RMSE), and coefficient of determination ( $R^2$ ). Statistical significance was assessed via paired Wilcoxon signed-rank tests<sup>109</sup>.

### III. RESULTS

#### A. Simulation-derived cohesive energies correlate with experimental boiling points across multiple force fields and temperatures

The boiling point of a substance is a direct manifestation of its intermolecular cohesive forces, a foundational principle of classical thermodynamics<sup>110</sup>. Based on this principle, we hypothesized that descriptors derived directly from the physics of the liquid phase could serve as a more robust foundation for property prediction than purely structural representations. Our approach therefore leverages cohesive energy, extracted directly from atomistic simulations, to encode the intermolecular interaction landscape that governs phase transitions, thereby avoiding reliance on predefined structural fragments or empirical group contributions.

To validate this hypothesis, our initial objective was to establish a direct, quantitative relationship between the computed cohesive energy and experimental boiling points. We perform atomistic molecular dynamics simulations of 1,280 organic compounds (see section II.B) at three temperatures (300, 400, and 500K). To interrogate the robustness of this physics-based descriptor, we compare the performance of two structurally distinct force fields: OpenFF-2.0.0<sup>97</sup>, a modern open-source parameterization, and OPLS4<sup>99</sup>, an extensively validated commercial force field, yielding a total of 7,680 independent trajectories (1,280 compounds  $\times$  3 temperatures  $\times$  2 force fields). As shown in Fig. 2, our analysis reveals a strong linear correlation between the simulated cohesive energy and experimental boiling points, though its quality is force-field dependent. This linear trend is physically grounded in Trouton’s rule, which implies a direct proportionality between the heat of vaporization ( $\Delta H_{\text{vap}}$ )—for which our cohesive energy is a proxy—and the boiling temperature ( $T_b$ )<sup>110</sup>. Under the OpenFF-2.0.0 force field (Fig. 2a), linear regression yields coefficients of determination ( $R^2$ ) of 0.73 (300 K; blue), 0.76 (400 K; green), and 0.73 (500 K; pink). This correlation is further en-

hanced with the OPLS4 force field (Fig. 2b), which affords  $R^2$  values of 0.77 (300 K), 0.81 (400 K), and 0.82 (500 K). More important than the performance difference is the fact that a strong correlation exists for both, especially considering that neither force field was parameterized using boiling points from this dataset. This demonstrates the robustness of cohesive energy as a physics-based descriptor; its utility is not an artifact of a single, specific parameterization but stems from the underlying physical principle it represents. Taken together, this extensive linear analysis confirms that our physics-based approach robustly captures the fundamental intermolecular interactions governing boiling behavior. However, the residual scatter indicates that a simple linear model is insufficient. This is physically expected, as a linear model implicitly assumes a constant entropy of vaporization ( $\Delta S_{\text{vap}}$ ) across all compounds (the basis of Trouton’s rule). The observed deviation from linearity thus arises from molecule-specific variations in this entropic contribution. This is precisely where a flexible, non-linear machine-learning model becomes essential, as it can learn the complex mapping from the enthalpic features to the final boiling point while implicitly accounting for these entropic variations.

A visible feature in both panels of Fig. 2 is the emergence of data points with cohesive energies approaching zero, most prominently at the higher simulation temperatures (400 K in green and 500 K in pink). These cases correspond to compounds that undergo vaporization during the NPT simulations, transitioning from a condensed liquid to a dilute gas phase; in this regime, molecules are separated by large distances, intermolecular interactions are negligible, and the computed cohesive energy tends toward zero. Thus, these systems exhibit sharply reduced densities and expanded simulation-box volumes characteristic of the gas state. Importantly, we deliberately retain these phase-transitioned trajectories in the training dataset: they provide explicit supervision linking thermodynamic descriptors—low  $E_{\text{coh}}$ , low density, high molar volume—to lower boiling points, and delineate the boundary where simulation-derived features remain physically meaningful. In practice, this exposure will enable the CatBoost<sup>92</sup> regressor to implicitly encode liquid–gas phase behavior, enhancing predictive capability for compounds spanning a broad range of volatilities.

#### B. Machine learning models trained on simulation-derived descriptors achieve competitive accuracy with substantially reduced feature dimensionality

Having verified that simulation-derived cohesive energies correlate strongly with experimental boiling points (Fig. 2), we next evaluate whether these thermodynamic descriptors can serve as effective features for machine learning prediction models. To this end, we trained three categories of CatBoost<sup>92</sup> gradient-boosted regression models (see Materials and Methods S.II.D for com-

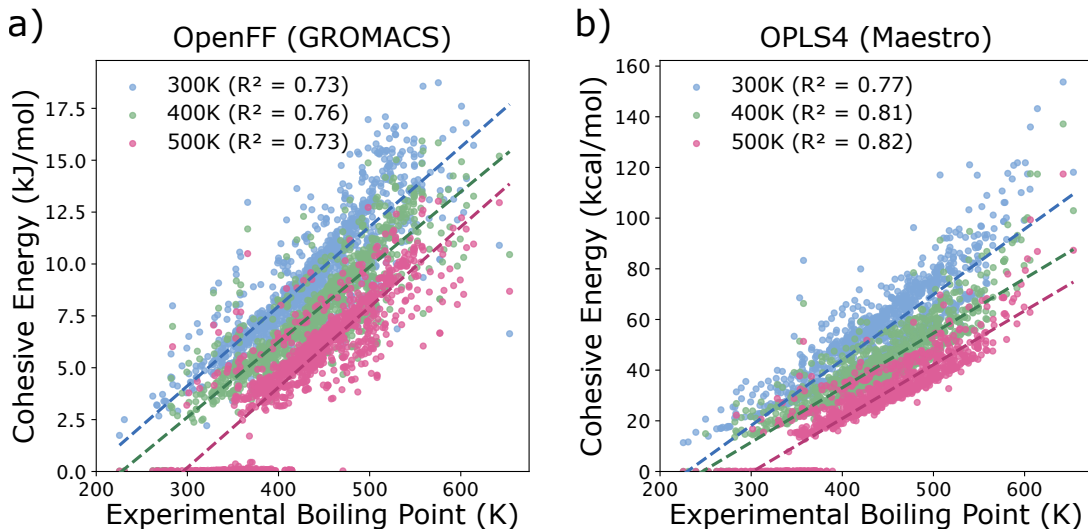


FIG. 2. Correlation between simulation-derived cohesive energy ( $E_{\text{coh}}$ ) and experimental boiling point ( $T_b$ ) for 1,280 organic compounds simulated at three temperatures using two independent force fields. (a) OpenFF-2.0.0<sup>97</sup> results showing linear relationships at 300 K (blue), 400 K (green), and 500 K (pink) with corresponding  $R^2$  values of 0.73, 0.76, and 0.73, respectively. (b) OPLS4<sup>99</sup> results at the same temperature conditions yielding  $R^2$  values of 0.77, 0.81, and 0.82. Each data point represents ensemble-averaged intermolecular interaction energies extracted from 20 ns NPT simulations. Data points at near-zero cohesive energy (predominantly at 500K) correspond to compounds that have undergone phase transition to the gas phase during simulation, exhibiting negligible intermolecular interactions due to substantial box expansion and reduced density. They are kept intentionally for the ML model to learn when MD features are meaningful. Linear regression lines are fitted to the full dataset at each temperature, encompassing both liquid-phase and transitioned gas-phase systems.

plete training details): (i) MD-only models using exclusively simulation-derived thermodynamic properties, (ii) cheminformatics-only models based on molecular fingerprints and 2D structural descriptors, and (iii) hybrid models combining both descriptor types.

Figure 3A presents the prediction performance of the MD-only models. This parity plot demonstrates that a model trained exclusively on a minimal set of thermodynamic features can yield remarkable predictive accuracy. The model trained on OPLS4-derived features (purple) achieves a strong coefficient of determination of  $R^2 = 0.95$ , closely tracking the line of perfect prediction. The model based on OpenFF-2.0.0 descriptors (yellow) also performs well, with an  $R^2 = 0.90$ , though the increased scatter underscores the sensitivity of the approach to force field parameterization, simulation engine and the specific thermostat and barostat algorithms employed in each workflow. The significant improvement in predictive power, moving from the linear correlations in (Fig. 2a and b) to the machine learning predictions in (Fig. 3), stems from the model’s ability to interpret complex, non-linear thermodynamic behavior. The points with near-zero cohesive energy that appeared as outliers relative to the linear trend in (Fig. 2) are no longer outliers here. The CatBoost regressor, unlike a simple linear model, successfully learns to associate the full thermodynamic signature of this gas-phase state with a low boiling point. This capability is a primary driver of the model’s high predictive accuracy.

To contextualize the performance of our MD-only

model, we conducted a systematic benchmark against the other architectures, presented in Figure 3B. The analysis reveals a clear performance hierarchy. Using the high-fidelity OPLS4 force field, the "MD+Chemoinf." hybrid model, which combines both MD and cheminformatics features, attains the highest accuracy with a mean absolute error (MAE) of 6.2K and a root mean squared error (RMSE) of 11.7K (dark green bar). It is closely followed by the "cheminformatics-only" model, trained on a high-dimensional feature set of over 2,000 descriptors, which achieves an MAE of 6.9K and an RMSE of 12.2K (teal bar). Strikingly, our MD-only model (dark blue bar) remains highly competitive with an MAE of 8.2K and an RMSE of 13.8K. This result is highly significant. By replacing thousands of abstract structural features with a handful of physically meaningful descriptors, we reduce the feature dimensionality by over two orders of magnitude. This dramatic reduction is a standard strategy to mitigating the risk of overfitting, as the model is encouraged to learn the governing physical principles rather than memorizing spurious correlations from the training data<sup>111,112</sup>. This, in turn, is fundamental to its enhanced extrapolative power. Remarkably, this robust generalization is achieved with only a minor sacrifice of 2K in MAE relative to the best-performing, high-dimensional model. The force field dependence is also instructive. The performance of the MD-only model is highly sensitive to the physical accuracy of the simulation, with the MAE degrading from 8.2K with OPLS4 to 12.2K with OpenFF-2.0.0 (hatched dark blue bar). In con-

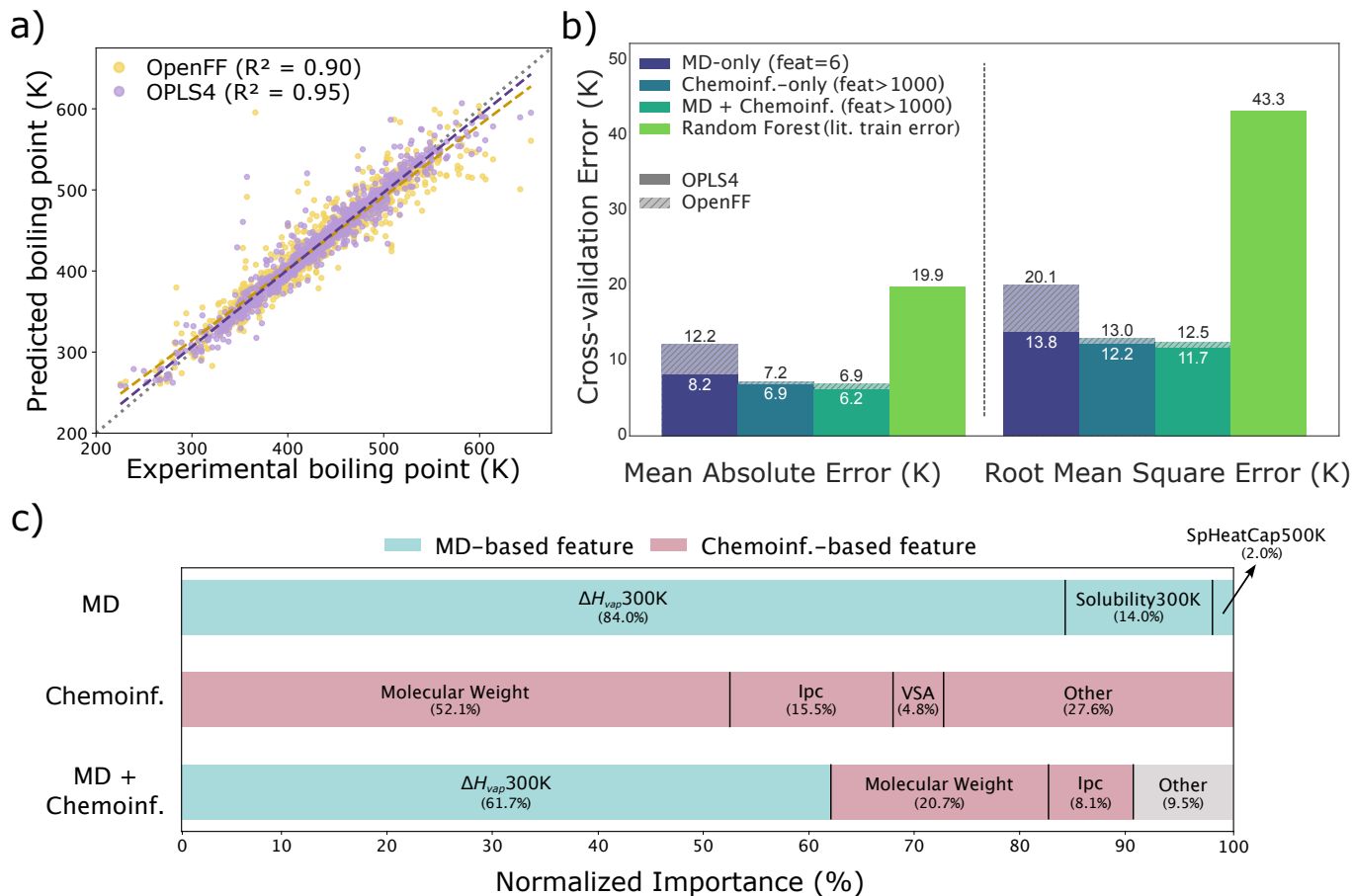


FIG. 3. Performance comparison of machine learning models trained on different descriptor sets for boiling point prediction. (a) Cross-validated predicted versus experimental boiling points for the MD-only models. The plot shows the out-of-sample predictions on the 1,280-compound training set, obtained from the 4-fold cross-validation procedure described in the methods. The models were trained exclusively on thermodynamic descriptors from simulations with the OPLS4 (purple) and OpenFF-2.0.0 (yellow) force fields. The solid black line represents a perfect prediction. (b) Cross-validated prediction errors across multiple model architectures. Bars represent mean absolute error (MAE) and root mean squared error (RMSE) for: MD-only models (dark blue), chemoinformatics-only models trained on molecular fingerprints and 2D descriptors (teal), hybrid models combining both descriptor types (dark green), and a literature baseline using Random Forest on the original uncurated dataset (light green)<sup>49</sup>. Solid bars correspond to OPLS4-derived features, while hatched bars show results for OpenFF-2.0.0 features. (c) Normalized feature importance (in %) for the OPLS4-based model architectures. The horizontal bars show the relative contribution of the most significant features. Blue segments represent MD-derived features red segments represent chemoinformatics descriptors, and gray represents the cumulative importance of other minor structural features. Top bar (MD-only, 3 features selected): Importance is concentrated in thermodynamic features like the heat of vaporization ( $\Delta H_{vap}$ ). Middle bar (Chemoinformatics-only, >1000 features used): Importance is led by molecular weight, followed by the information content of the characteristic polynomial (Ipc) and van der Waals surface area (VSA). Bottom bar (Hybrid, >1000 features used): A synergistic model where a thermodynamic features are complemented by key structural descriptors.

trast, the hybrid model shows remarkable resilience, with its MAE only slightly increasing from 6.2K (OPLS4) to 6.9K (OpenFF). This suggests that structural descriptors can partially compensate for inaccuracies in simulation-derived properties, providing a practical pathway for deployment. For a final point of comparison, we include results from the Random Forest model reported by Kim et al.<sup>49</sup>, the study from which our initial, uncurated dataset was sourced (light green bar) (see section S.II.A for more details about the data). This baseline model exhibits substantially higher errors (MAE = 19.9K, RMSE =

43.3K) than even our worst-performing variant. Several factors likely contribute to this performance gap. We hypothesize that two primary factors are: (i) our rigorous data curation produced a cleaner, more consistent training set, and (ii) our physics-based descriptors provide more causally relevant information than purely structural features. However, it must be acknowledged that a third confounding variable is the change in the learning algorithm itself, from a Random Forest to a CatBoost model, which may also contribute to the observed improvement. A full deconvolution of these effects is beyond the scope

of this study.

A deep dive into the feature importance, visualized in Figure 3C, reveals the distinct predictive logic of each model and highlights the efficiency of the physics-informed approach. Here, MD-derived features are colored in blue and chemoinformatics descriptors in red. For the MD-only model (top bar), we initially provided a pool of 15 physics-based features: five thermodynamic properties—cohesive energy ( $E_{\text{coh}}$ ), heat of vaporization ( $\Delta H_{\text{vap}}$ ), density ( $\rho$ ), solubility parameter ( $\delta$ ), and isobaric specific heat capacity ( $C_P$ )—each calculated at three different temperatures (see section S.II.B for further details). From this set, CatBoost’s internal feature selection algorithm identifies the most predictive, non-redundant subset. For the model trained on the OPLS4 data, we observe a highly compact feature selection, with the model identifying just three features as sufficient for optimal prediction. As shown in the top bar, the predictive power is overwhelmingly concentrated in the heat of vaporization at 300K ( $\Delta H_{\text{vap}300\text{K}}$ ), which accounts for 84% of the model’s cumulative feature importance. The solubility parameter ( $\delta$ ) at 300K (Solubility300K, 14%) and specific heat capacity at 500K (SpHeatCap500K, 2%) play minor, supporting roles. This specific three-feature selection, however, highlights the model’s data-driven nature rather than a fixed physical rule. The algorithm’s goal is to find the most predictive signal, and the composition of that signal is force-field dependent. For instance, when the same modeling process is applied to the features derived from the OpenFF simulations (see Supplementary Information, Fig.S1 in Supplementary Information), the model selects a larger and more varied set of six features. This is instructive, suggesting that for the OpenFF-derived data, the predictive signal is more distributed across several thermodynamic properties, prompting the algorithm to construct a more complex model to capture it effectively. What remains consistent is the flexibility of our strategy: the model successfully mines the available thermodynamic data, adapting its feature selection to the specific physical representation provided by each force field.

In contrast, the chemoinformatics-based models leverage over 1000 features, but their importance distribution is revealing. In the chemoinformatics-only model, importance is led by molecular weight (52.1%), but a substantial portion (27.6%) is fragmented across a vast "long tail" of abstract structural descriptors. This stark contrast in the number of employed features—a handful of physical properties versus over a thousand abstract ones—is a central finding of our work. The hybrid model, however, reveals the decisive influence of the physics-augmented features. In the OPLS4-based model, a single thermodynamic descriptor—the heat of vaporization at 300K ( $\Delta H_{\text{vap}}$ )—emerges as the overwhelmingly dominant feature, accounting for 61.7% of the total importance. This single physical property is nearly three times as important as the next most significant feature, molecular weight (20.7%), proving it provides the core

predictive signal, which is then refined by structural information. This dominance of MD-derived features as the most significant predictive block is consistent across both force fields (see Supplementary Information, Fig.S1).

Together, these results establish a powerful principle: the computational investment in generating simulation-derived thermodynamic properties pays significant dividends in predictive power and interpretability. The ability of the MD-only model to distill the prediction down to a few physically intuitive features like  $\Delta H_{\text{vap}}$ , marks a conceptual advance. This approach transcends the 'black-box' correlation of abstract features by establishing a direct link between the target property and its underlying physical causes. This pursuit of interpretability and causal reasoning is a central goal of modern scientific machine learning<sup>113,114</sup>. This work, therefore, not only delivers a high-performance predictive tool but also provides strong support for the development of machine learning models for chemistry that are anchored in first principles based inputs to enhance robustness.

### C. MD-based models demonstrate superior extrapolation to structurally novel and complex chemical systems

Given the superior performance of the models trained on OPLS4-derived features, as demonstrated in the previous section, we selected these specific models for the subsequent extrapolation and benchmarking tests. A critical measure of a machine learning model’s utility is not just its accuracy within its training domain, but its ability to generalize to new, structurally distinct chemical matter. This capability is of crucial relevance for industrial applications in the pharmaceutical, crop science, and chemical sectors, where the exploration of novel molecular structures is essential for generating intellectual property and discovering materials with unprecedented properties. To evaluate the extrapolative power of our approach, we benchmarked our models against several well-established boiling point predictors: the group-contribution-based Joback<sup>31</sup> and Rarey-Nannoolal<sup>32</sup> methods, as well as a state-of-the-art graph neural network, GRAPPA<sup>66</sup>. A key factor in this selection was their practical accessibility via public web tools that provide instantaneous predictions directly from a SMILES string, such as those for Joback<sup>115</sup> and GRAPPA<sup>116</sup>, allowing for a reproducible benchmark. The benchmark was performed on our rigorous external benchmark set (see section S.II.A). This set was deliberately curated to probe the limits of extrapolation and consists of 32 structurally diverse active pharmaceutical ingredients with varied complexity sourced from the DrugBank database<sup>96</sup>. These molecules were chosen to represent the kind of structurally complex, real-world chemical matter encountered in industrial discovery pipelines. Crucially, while complex, they are composed of standard organic elements, placing them squarely within the theoretical applicability domain of the chemoinformatic predictors we benchmark. This de-

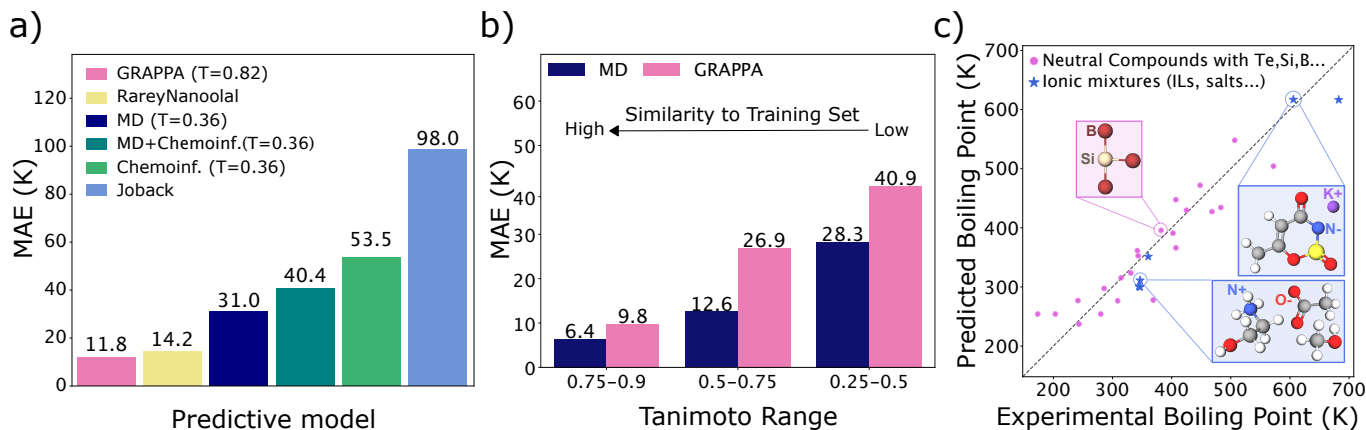


FIG. 4. Extrapolative performance of MD-based models on structurally novel and complex chemical systems. (a) Mean Absolute Error (MAE) on a curated test set of 32 complex organic molecules for various models: GRAPPA (pink), Rarey-Nanolal (yellow), MD-only (dark blue), hybrid MD+chemoinformatics (dark green), chemoinformatics-only (light green), and the Joback method (light blue). The average Tanimoto similarity of the test set to the respective training sets is noted for GRAPPA (0.82) and our models (0.38), highlighting the greater novelty of the test set for our approach. (b) MAE comparison between the MD-only model (dark blue) and GRAPPA (pink), stratified by Tanimoto similarity between test compounds and each model’s respective training set. The MD-only model demonstrates consistently lower error, with its advantage growing significantly as structural similarity decreases. Each bin contains at least 3 data points. (c) Predicted versus experimental boiling points for chemical systems outside the applicability domain of most existing predictors. The model successfully predicts boiling points for neutral compounds with uncommon elements like Si, B, and Te (pink circles, e.g., tribromosilane) and charged systems including salts and ionic liquids (blue stars, e.g., Acesulfame K and an IL-methanol mixture).

sign ensures a direct and fair head-to-head comparison of true extrapolative performance, with the data also being curated to ensure high-quality experimental values and compatibility across all models. It is important to note the practical trade-off between predictive speed and extrapolative power. While chemoinformatic models are instantaneous, our physics-augmented approach requires an upfront simulation step. However, this computational cost is modest and highly accessible. On a modern GPU, a 20 ns simulation for a single compound is typically completed in 3-4 hours. Even on standard CPUs, the task takes approximately 15-20 hours using only 2 cores. This makes it feasible to generate descriptors for dozens of compounds simultaneously on a modern multi-core workstation or a small high-performance computing cluster, representing a practical and manageable investment to unlock the model’s robust extrapolative capabilities.

Figure 4A plots the Mean Absolute Error (MAE) in Kelvin for all models on this challenging extrapolation test set. The corresponding Root Mean Squared Error (RMSE) plot, which reinforces the same trends, is provided in the Supplementary Information (Fig.S2.A). A surface-level comparison of the MAE suggests that the literature models GRAPPA and Rarey-Nanolal achieve the highest accuracy. However, this comparison requires careful contextualization. GRAPPA’s high performance is likely attributable to its strength in interpolation, given its vast training set of 20,000 compounds. A Tanimoto similarity analysis supports this view. While the Tanimoto coefficient is a simple heuristic for molecular similarity, in this case it effectively delineates the

domain of applicability. The test set compounds exhibit a high average similarity of 0.82 to GRAPPA’s training set, but a low similarity (0.38) to our own. This confirms that for our models, this benchmark represents a significantly more challenging “out-of-distribution” extrapolation task.

Importantly, this out-of-distribution challenge reveals a complete reversal of the performance hierarchy observed during interpolation. As seen in Figure 4A, our MD-only model now clearly outperforms the other models trained in this work, with an MAE of 31.0K. This result highlights a known limitation of chemoinformatics descriptors: features that are effective for interpolating within a known chemical space become unreliable when the model is faced with novel structures containing fragments or motifs absent from the training data<sup>117</sup>. The performance degradation is systematic: the chemoinformatics-only model fails (MAE = 53.5K), and the hybrid model (MAE = 40.4K) is penalized by the inclusion of these same unreliable structural features. In its own right, a model like GRAPPA provides fast, high-precision predictions and remains the superior tool within its well-defined domain. However, our results clearly show that for true out-of-distribution extrapolation, a model anchored in the underlying physics is fundamentally more robust. This finding aligns with recent conclusions in other domains, such as protein-ligand binding affinity prediction<sup>118</sup>.

The success of GRAPPA<sup>66</sup> in the initial benchmark demanded a more granular, head-to-head comparison to dissect the true generalization capabilities of both our

MD-only model and the GNN. To achieve this, we stratified the external test set by Tanimoto similarity, measuring how structurally similar each test compound is to its nearest neighbor in each model’s respective training set (a full breakdown is provided in S.I of Supplementary Information). This analysis (Fig.S2.B) reveals their fundamentally different strengths. In the high-similarity regime (Tanimoto  $\geq$  0.95), GRAPPA’s performance is exceptional, with its MAE dropping to 4.1K for compounds most similar to its training data, confirming its power as a high-precision interpolator. To assess true extrapolative capability, we therefore focused the main analysis on the more challenging similarity range below 0.9 (Fig. 4B). In this view, a clear and consistent trend emerges where our MD-only model maintains a superior performance. For compounds with moderate similarity (0.75–0.9), our model’s MAE is 6.4K versus 9.8K for GRAPPA. This performance gap widens substantially as compound novelty increases, with our model achieving an MAE of 12.6K versus 26.9K in the medium similarity range, and 28.3K versus 40.9K for the most dissimilar compounds.

The contrast in robustness becomes even more stark when normalizing the performance against each model’s own optimal baseline. GRAPPA’s error escalates from its 4.1K interpolation baseline by a factor of approximately 10 to predict the most dissimilar compounds. In stark contrast, our MD-only model exhibits a far more controlled response, with its MAE growing from its own 6.4K baseline by a factor of only 4.4 in the same low-similarity regime. This analysis confirms their distinct predictive behaviors: while GRAPPA excels at high-precision interpolation, our physics-informed model demonstrates a more graceful and predictable degradation of performance when faced with structural novelty. These results validate the physics-augmented strategy as a robust foundation for building more reliable predictive tools, particularly for the challenging low-similarity regime where traditional models falter.

The ultimate advantage of a physics-based approach is the ability to predict properties for chemical classes that lie entirely outside the domain of traditional models. Many existing predictors, including GRAPPA, are restricted to neutral organic molecules containing a limited set of elements (typically C, H, O, N, S, P, and sometimes various halogens) and cannot handle charged species or exotic elements. Our MD-based framework has no such intrinsic limitations. Fig. 4C showcases the model’s capability to extrapolate to these systems even though they were not in the training set. The first group (pink circles) includes neutral compounds containing uncommon elements such as Si, B, and Te, or molecules lacking carbon altogether (e.g., tribromosilane). The second group (blue stars) comprises charged systems, including salts (e.g., Acesulfame K), ionic liquids (ILs), and ternary mixtures containing ILs and solvents. We note that compiling this validation set required extensive literature curation, as reliable, experimentally measured boiling points for such systems are scarce, particularly for salts and ILs which

often decompose at high temperatures<sup>119</sup>. The ability of our model to make reasonable predictions for these complex systems, which are inaccessible to many widely used tools, underscores the power of leveraging fundamental thermodynamic properties for molecular property prediction and opens a path toward a more universal predictive framework.

Taken together, this section thus demonstrates the distinct advantages of a thermodynamics-informed framework: it is more robust for extrapolation towards new structures and elemental compositions and enables prediction for chemical domains, such as inorganic and charged species, that lie beyond the reach of conventional methods.

#### IV. CONCLUSIONS

In this work, we have developed a physics-augmented machine learning framework that demonstrates how first-principles-informed networks can perform more robustly when extrapolating. While existing methods like the group contribution-based Rarey-Nannoolal<sup>32</sup> or machine learning models like GRAPPA<sup>66</sup> are competitive, our work highlights a specific strength in navigating structural novelty. Our approach successfully integrates the regression power of modern machine learning with the fundamental principles of thermodynamics and explicit MD simulations, offering a complementary tool for exploring the novel chemical spaces.

Our first critical step was to validate the physical premise of our approach, establishing a strong, direct correlation between simulated cohesive energies and experimental boiling points across multiple force fields and temperatures (Fig. 2). Building on this, we demonstrated that a minimal set of just three simulation-derived features—principally the heat of vaporization—is sufficient to build an "MD-only" model with predictive accuracy competitive with complex cheminformatics models that rely on thousands of abstract descriptors (Fig. 3B). This constitutes a feature dimensionality reduction of over two orders of magnitude, transforming the prediction from a "black-box" exercise into an interpretable, physically-grounded regression. The model’s reliance on  $\Delta H_{\text{vap}}$  confirms it learns the correct underlying physics, a level of transparency that purely structural models lack.

The primary strength of our framework is revealed when venturing beyond familiar chemical territory. Our physics-informed model’s performance is substantially less sensitive to growing structural dissimilarity, a stark contrast to the brittleness of purely data-driven approaches (Fig. 4A-B). This robustness establishes our model as a reliable complementary tool, capable of predicting boiling points for systems inaccessible to most established methods, including inorganic compounds, molecules with uncommon elements like silicon and boron, and charged systems such as ionic liquids

(Fig. 4C). By anchoring predictions to fundamental thermodynamics, we demonstrate a clear path toward more generalizable ML models capable of navigating uncharted chemical space.

While this study is focused solely on normal boiling point predictions, our results provide strong, systematic evidence for a broader principle: MD-informed machine learning models are more robust for predicting condensed-phase properties governed by intermolecular forces. The framework presented here is not a single-purpose solution but a promising research direction. Rooting predictions in thermodynamics offers a pathway to develop more accurate and widely applicable models, essential for navigating the unexplored chemical territories vital to the future of materials science, pharmacology, drug discovery and engineering.

## V. ACKNOWLEDGEMENTS

N.H.E. acknowledges funding from Bayer Aktiengesellschaft, Division CropScience residing at Kaiser-Wilhelm-Allee 1, 51373 Leverkusen, Germany (“Bayer”). J.R. acknowledges funding from the Spanish Ministry of Economy and Competitiveness (PID2022-136919NB-C32). J.R.E. acknowledges funding from Emmanuel College, the University of Cambridge, the Ramon y Cajal fellowship (RYC2021-030937-I), the Spanish scientific plan and committee for research reference PID2022-136919NA-C33, and the European Research Council (ERC) under the European Union’s Horizon Europe research and innovation program (grant agreement no. 101160499). This work has been performed using resources provided by the HPC system in Bayer. The authors also thankfully acknowledge RES computational resources provided by Mare Nostrum 5 through the activity 2024-3-0001. Finally, the authors thank Marco Hoffmann for generously providing GRAPPA’s training set data, which enabled a direct and valuable comparison between models.

## VI. DATA AVAILABILITY

To ensure the reproducibility of our research, all relevant data, simulation parameters, and analysis scripts have been deposited in a [public GitHub repository](#). The repository contains the three datasets used in this work, as detailed in the Materials and Methods section. Furthermore, it provides the GROMACS input files (.mdp) for the energy minimization and production steps of the molecular dynamics simulations based on the OpenFF toolkit.

## VII. REFERENCES

<sup>1</sup>G. Schneider, “Automating drug discovery,” *Nature reviews drug discovery* **17**, 97–113 (2018).

- <sup>2</sup>K.-K. Mak, Y.-H. Wong, and M. R. Pichika, “Artificial intelligence in drug discovery and development,” *Drug discovery and evaluation: safety and pharmacokinetic assays*, 1461–1498 (2024).
- <sup>3</sup>H. Van De Waterbeemd and E. Gifford, “Admet in silico modelling: towards prediction paradise?” *Nature reviews Drug discovery* **2**, 192–204 (2003).
- <sup>4</sup>R. C. Reid, T. K. Sherwood, and R. E. Street, “The properties of gases and liquids,” *Physics Today* **12**, 38–40 (1959).
- <sup>5</sup>L. M. Egolf, M. D. Wessel, and P. C. Jurs, “Prediction of boiling points and critical temperatures of industrially important organic compounds from molecular structure,” *Journal of Chemical Information and Computer Sciences* **34**, 947–956 (1994).
- <sup>6</sup>J. D. Seader, E. J. Henley, and D. K. Roper, “Separation process principles: Chemical and biochemical operations,” John Wiley & Sons (2016).
- <sup>7</sup>P. G. Jessop, “Searching for green solvents,” *Green Chemistry* **13**, 1391–1398 (2011).
- <sup>8</sup>D. Prat, A. Wells, J. Hayler, H. Sneddon, C. R. McElroy, S. Abou-Shehada, and P. J. Dunn, “Cyanex solvent selection guide,” *Green Chemistry* **18**, 288–296 (2016).
- <sup>9</sup>B. E. Poling, J. M. Prausnitz, and J. P. O’Connell, *The Properties of Gases and Liquids*, 5th ed. (McGraw-Hill, New York, 2001).
- <sup>10</sup>I. H. Bell, J. Wronski, S. Quoilin, and V. Lemort, “Pure and pseudo-pure fluid thermophysical property evaluation and the open-source thermophysical property library coolprop,” *Industrial & Engineering Chemistry Research* **53**, 2498–2508 (2014).
- <sup>11</sup>S. Kim, J. Chen, T. Cheng, A. Gindulyte, J. He, S. He, Q. Li, B. A. Shoemaker, P. A. Thiessen, B. Yu, *et al.*, “Pubchem 2025 update,” *Nucleic acids research* **53**, D1516–D1525 (2025).
- <sup>12</sup>S. I. Sandler, *Chemical, Biochemical, and Engineering Thermodynamics*, 5th ed. (John Wiley & Sons, 2017).
- <sup>13</sup>W. Wu, R. Sayin, K. Shvedova, S. C. Born, C. J. Testa, S. S. Yeole, A. S. Censullo, A. K. Srivastava, A. Ramnath, C. Hu, *et al.*, “A continuous rotary filtration for the separation and purification of an active pharmaceutical ingredient,” *Organic Process Research & Development* **28**, 1618–1631 (2023).
- <sup>14</sup>A. Castro, I. Sanchez-Burgos, N. H. Espejo, A. Garaizar, G. M. Maggioni, and J. R. Espinosa, “Understanding how synthetic impurities affect glyphosate solubility and crystal growth using free energy calculations and molecular dynamics simulations,” *The Journal of Physical Chemistry B* (2025).
- <sup>15</sup>C. Finotti Cordeiro, L. Lopardi Franco, D. Teixeira Carvalho, and R. Bonfilio, “Impurities in active pharmaceutical ingredients and drug products: A critical review,” *Critical Reviews in Analytical Chemistry* **56**, 55–75 (2026).
- <sup>16</sup>J. F. Brennecke and E. J. Maginn, “Ionic liquids: innovative fluids for chemical processing,” *American Institute of Chemical Engineers. AIChE Journal* **47**, 2384 (2001).
- <sup>17</sup>J.-C. De Hemptinne, G. M. Kontogeorgis, R. Dohrn, I. G. Economou, A. Ten Kate, S. Kuitunen, L. Fele Žilnik, M. G. De Angelis, and V. Vesovic, “A view on the future of applied thermodynamics,” *Industrial & Engineering Chemistry Research* **61**, 14664–14680 (2022).
- <sup>18</sup>B. I. Lee and M. G. Kesler, “A generalized thermodynamic correlation based on three-parameter corresponding states,” *AIChE Journal* **21**, 510–527 (1975).
- <sup>19</sup>D. Ambrose and J. Walton, “Vapour pressures up to their critical temperatures of normal alkanes and 1-alkanols,” *Pure and Applied Chemistry* **61**, 1395–1403 (1989).
- <sup>20</sup>B. E. Poling, J. M. Prausnitz, and O. John Paul, *The properties of gases and liquids* (McGraw-Hill New York, 2001).
- <sup>21</sup>D. Edwards and J. Prausnitz, “Estimation of vapor pressures of heavy liquid hydrocarbons containing nitrogen or sulfur by a group-contribution method,” *Industrial & Engineering Chemistry Fundamentals* **20**, 280–283 (1981).
- <sup>22</sup>C.-H. Tu, “Group-contribution method for the estimation of vapor pressures,” *Fluid Phase Equilibria* **99**, 105–120 (1994).

- <sup>23</sup>L. Constantinou and R. Gani, "New group contribution method for estimating properties of pure compounds," *AIChE Journal* **40**, 1697–1710 (1994).
- <sup>24</sup>J. Marrero-Morejón and E. Pardillo-Fontdevila, "Estimation of pure compound properties using group-interaction contributions," *AIChE journal* **45**, 615–621 (1999).
- <sup>25</sup>W. E. Asher and J. F. Pankow, "Vapor pressure prediction for alkenoic and aromatic organic compounds by a unific-based group contribution method," *Atmospheric Environment* **40**, 3588–3600 (2006).
- <sup>26</sup>J. F. Pankow and W. E. Asher, "Simpol. 1: a simple group contribution method for predicting vapor pressures and enthalpies of vaporization of multifunctional organic compounds," *Atmospheric Chemistry and Physics* **8**, 2773–2796 (2008).
- <sup>27</sup>B. Moller, J. Rarey, and D. Ramjugernath, "Estimation of the vapour pressure of non-electrolyte organic compounds via group contributions and group interactions," *Journal of Molecular Liquids* **143**, 52–63 (2008).
- <sup>28</sup>R. Ceriani, R. Gani, and Y. Liu, "Prediction of vapor pressure and heats of vaporization of edible oil/fat compounds by group contribution," *Fluid Phase Equilibria* **337**, 53–59 (2013).
- <sup>29</sup>M. Rezakazemi, A. Marjani, and S. Shirazian, "Development of a group contribution method based on unific groups for the estimation of vapor pressures of pure hydrocarbon compounds," *Chemical Engineering & Technology* **36**, 483–491 (2013).
- <sup>30</sup>T.-Y. Wang, X.-Z. Meng, M. Jia, and X.-C. Song, "Predicting the vapor pressure of fatty acid esters in biodiesel by group contribution method," *Fuel Processing Technology* **131**, 223–229 (2015).
- <sup>31</sup>K. G. Joback and R. C. Reid, "Estimation of pure-component properties from group-contributions," *Chemical Engineering Communications* **57**, 233–243 (1987).
- <sup>32</sup>Y. Nannoolal, J. Rarey, D. Ramjugernath, and W. Cordes, "Estimation of pure component properties: Part 1. estimation of the normal boiling point of non-electrolyte organic compounds via group contributions and group interactions," *Fluid Phase Equilibria* **226**, 45–63 (2004).
- <sup>33</sup>A. Alibakhshi and B. Hartke, "Dependence of vaporization enthalpy on molecular surfaces and temperature: Thermodynamically effective molecular surfaces," *Physical Review Letters* **129**, 206001 (2022).
- <sup>34</sup>D.-Y. Peng and D. B. Robinson, "A new two-constant equation of state," *Industrial & Engineering Chemistry Fundamentals* **15**, 59–64 (1976).
- <sup>35</sup>W. G. Chapman, K. E. Gubbins, G. Jackson, and M. Radosz, "Saft: Equation-of-state solution model for associating fluids," *Fluid Phase Equilibria* **52**, 31–38 (1989).
- <sup>36</sup>J. Gross and G. Sadowski, "Perturbed-chain saft: An equation of state based on a perturbation theory for chain molecules," *Industrial & engineering chemistry research* **40**, 1244–1260 (2001).
- <sup>37</sup>A. Klamt and F. Eckert, "Cosmo-rs: a novel and efficient method for the a priori prediction of thermophysical data of liquids," *Fluid Phase Equilibria* **172**, 43–72 (2000).
- <sup>38</sup>M. Zhang and E. M. Suuberg, "Estimation of vapor pressures of perfluoroalkyl substances (pfas) using cosmo-therm," *Journal of Hazardous Materials* **443**, 130185 (2023).
- <sup>39</sup>C. Song, R. Shariyati, and I. Alkhrsan, "Prediction of thermodynamic properties of ionic liquids using the pc-saft eos coupled with cosmo-rs model," *Chemical Engineering Research and Design* **213**, 1–10 (2025).
- <sup>40</sup>T. Dupeux, T. Gaudin, C. Marteau-Roussy, J.-M. Aubry, and V. Nardello-Rataj, "Cosmo-rs as an effective tool for predicting the physicochemical properties of fragrance raw materials," *Flavour and Fragrance Journal* **37**, 106–120 (2022).
- <sup>41</sup>K. A. Kurnia, S. P. Pinho, and J. A. Coutinho, "Evaluation of the conductor-like screening model for real solvents for the prediction of the water activity coefficient at infinite dilution in ionic liquids," *Industrial & Engineering Chemistry Research* **53**, 12466–12475 (2014).
- <sup>42</sup>K. Padaszyński, "An overview of the performance of the cosmo-rs approach in predicting the activity coefficients of molecular solutes in ionic liquids and derived properties at infinite dilution," *Physical Chemistry Chemical Physics* **19**, 11835–11850 (2017).
- <sup>43</sup>A. R. Katritzky, V. S. Lobanov, and M. Karelson, "Qspr: the correlation and quantitative prediction of chemical and physical properties from structure," *Chemical Society Reviews* **24**, 279–287 (1995).
- <sup>44</sup>A. R. Katritzky, S. H. Slavov, D. A. Dobchev, and M. Karelson, "Rapid qspr model development technique for prediction of vapor pressure of organic compounds," *Computers & chemical engineering* **31**, 1123–1130 (2007).
- <sup>45</sup>S. Hilal, S. Karickhoff, and L. Carreira, "Prediction of the vapor pressure boiling point, heat of vaporization and diffusion coefficient of organic compounds," *QSAR & Combinatorial Science* **22**, 565–574 (2003).
- <sup>46</sup>Y. Dai, Z. Zhu, C. Zhong, Y. Zhang, J. Zeng, and L. Xun, "Prediction of boiling points of organic compounds by qspr tools," *Journal of Molecular Graphics and Modelling* **44**, 113–119 (2013).
- <sup>47</sup>H. Mirshahvalad, R. Ghasemiasl, N. Raoufi, and M. Malekzadeh Dirin, "A neural network qspr model for accurate prediction of flash point of pure hydrocarbons," *Molecular Informatics* **38**, 1800094 (2019).
- <sup>48</sup>M. R. Fissa, Y. Lahiouel, L. Khaouane, and S. Hanini, "Qspr estimation models of normal boiling point and relative liquid density of pure hydrocarbons using mlr and mlp-ann methods," *Journal of Molecular Graphics and Modelling* **87**, 109–120 (2019).
- <sup>49</sup>S.-Y. Kim, I. Jeon, and S.-J. Kang, "Integrating data science and machine learning to chemistry education: Predicting classification and boiling point of compounds," *Journal of Chemical Education* **101**, 1771–1776 (2024).
- <sup>50</sup>J.-h. Zhang, Z.-m. Liu, and W.-r. Liu, "Qspr study for prediction of boiling points of 2475 organic compounds using stochastic gradient boosting," *Journal of Chemometrics* **28**, 161–167 (2014).
- <sup>51</sup>A. N. Koam, M. U. Majeed, S. Zaman, A. Ahmad, I. Masmali, and A. A. H. Ahmadini, "Machine learning approaches for modeling the physicochemical characteristics of polycyclic aromatic hydrocarbons," *The European Physical Journal E* **48**, 21 (2025).
- <sup>52</sup>D. K. Duvenaud, D. Maclaurin, J. Iparraguirre, R. Bombarell, T. Hirzel, A. Aspuru-Guzik, and R. P. Adams, "Convolutional neural networks on graphs for learning molecular fingerprints," *Advances in neural information processing systems* **28** (2015).
- <sup>53</sup>J. Gilmer, S. S. Schoenholz, P. F. Riley, O. Vinyals, and G. E. Dahl, "Neural message passing for quantum chemistry," in *Proceedings of the 34th International Conference on Machine Learning*, Proceedings of Machine Learning Research, Vol. 70 (PMLR, 2017) pp. 1263–1272.
- <sup>54</sup>Z. Xiong, D. Wang, X. Liu, F. Zhong, X. Wan, X. Li, Z. Li, X. Luo, K. Chen, H. Jiang, *et al.*, "Pushing the boundaries of molecular representation for drug discovery with the graph attention mechanism," *Journal of medicinal chemistry* **63**, 8749–8760 (2019).
- <sup>55</sup>J. G. Rittig, K. C. Felton, A. A. Lapkin, and A. Mitsos, "Gibbs-duhem-informed neural networks for binary activity coefficient prediction," *Digital Discovery* **2**, 1752–1767 (2023).
- <sup>56</sup>J. Damay, F. Jirasek, M. Kloft, M. Bortz, and H. Hasse, "Predicting activity coefficients at infinite dilution for varying temperatures by matrix completion," *Industrial & Engineering Chemistry Research* **60**, 14564–14578 (2021).
- <sup>57</sup>T. Specht, M. Nagda, S. Fellenz, S. Mandt, H. Hasse, and F. Jirasek, "Hanna: hard-constraint neural network for consistent activity coefficient prediction," *Chemical science* **15**, 19777–19786 (2024).
- <sup>58</sup>W. Ahmad, H. Tayara, and K. T. Chong, "Attention-based graph neural network for molecular solubility prediction," *ACS omega* **8**, 3236–3244 (2023).

- <sup>59</sup>B. Winter, P. Rehner, T. Esper, J. Schilling, and A. Bardow, "Understanding the language of molecules: predicting pure component parameters for the pc-saft equation of state from smiles," *Digital Discovery* **4**, 1142–1157 (2025).
- <sup>60</sup>K. C. Felton, L. Raßpe-Lange, J. G. Rittig, K. Leonhard, A. Mitsos, J. Meyer-Kirschner, C. Knösche, and A. A. Lapkin, "ML-saft: A machine learning framework for pcp-saft parameter prediction," *Chemical Engineering Journal* **492**, 151999 (2024).
- <sup>61</sup>J. Habicht, C. Brandenbusch, and G. Sadowski, "Predicting pc-saft pure-component parameters by machine learning using a molecular fingerprint as key input," *Fluid Phase Equilibria* **565**, 113657 (2023).
- <sup>62</sup>C. Qu, A. J. Kearsley, B. I. Schneider, W. Keyrouz, and T. C. Allison, "Graph convolutional neural network applied to the prediction of normal boiling point," *Journal of Molecular Graphics and Modelling* **112**, 108149 (2022).
- <sup>63</sup>S. A. R. Sangala and S. Raghunathan, "Graph neural network for 3-dimensional structures including dihedral angles for molecular property prediction," *Journal of Computational Chemistry* **46**, e70121 (2025).
- <sup>64</sup>Y.-H. Lin, H.-H. Liang, S.-T. Lin, and Y.-P. Li, "Advancing vapor pressure prediction: A machine learning approach with directed message passing neural networks," *Journal of the Taiwan Institute of Chemical Engineers*, 105926 (2024).
- <sup>65</sup>V. V. Santana, C. M. Rebello, L. P. Queiroz, A. M. Ribeiro, N. Shardt, and I. B. Nogueira, "Puffin: A path-unifying feed-forward interfaced network for vapor pressure prediction," *Chemical Engineering Science* **286**, 119623 (2024).
- <sup>66</sup>M. Hoffmann, H. Hasse, and F. Jirasek, "Grappa—a hybrid graph neural network for predicting pure component vapor pressures," *Chemical Engineering Journal Advances* **22**, 100750 (2025).
- <sup>67</sup>J. G. Rittig, K. B. Hicham, A. M. Schweidtmann, M. Dahmen, and A. Mitsos, "Graph neural networks for temperature-dependent activity coefficient prediction of solutes in ionic liquids," *Computers & Chemical Engineering* **171**, 108153 (2023).
- <sup>68</sup>K. Yang, K. Swanson, W. Jin, C. Coley, P. Eiden, H. Gao, A. Guzman-Perez, T. Hopper, B. Kelley, M. Mathea, *et al.*, "Analyzing learned molecular representations for property prediction," *Journal of chemical information and modeling* **59**, 3370–3388 (2019).
- <sup>69</sup>I. V. Tetko, P. Karpov, R. Van Deursen, and G. Godin, "State-of-the-art augmented nlp transformer models for direct and single-step retrosynthesis," *Nature Communications* **11**, 5575 (2020).
- <sup>70</sup>J. P. Janet, S. Ramesh, C. Duan, and H. J. Kulik, "Accurate multiobjective design in a space of millions of transition metal complexes with neural-network-driven efficient global optimization," *ACS Central Science* **6**, 513–524 (2020).
- <sup>71</sup>Z. Wu, B. Ramsundar, E. N. Feinberg, J. Gomes, C. Geniesse, A. S. Pappu, K. Leswing, and V. Pande, "Moleculenet: a benchmark for molecular machine learning," *Chemical science* **9**, 513–530 (2018).
- <sup>72</sup>S. Gugler, *Machine learning with physics-based descriptors for quantum chemistry*, Ph.D. thesis, ETH Zurich (2023).
- <sup>73</sup>R. A. Bryce, "Physics-based scoring of protein–ligand interactions: explicit polarizability, quantum mechanics and free energies," *Future Medicinal Chemistry* **3**, 683–698 (2011).
- <sup>74</sup>S.-C. Li, H. Wu, A. Menon, K. A. Spiekermann, Y.-P. Li, and W. H. Green, "When do quantum mechanical descriptors help graph neural networks to predict chemical properties?" *Journal of the American Chemical Society* **146**, 23103–23120 (2024).
- <sup>75</sup>D. Frenkel and B. Smit, *Understanding Molecular Simulation: From Algorithms to Applications*, 2nd ed. (Academic Press, San Diego, 2002).
- <sup>76</sup>T. Köddermann, D. Paschek, and R. Ludwig, "Molecular dynamic simulations of ionic liquids: A reliable description of structure, thermodynamics and dynamics," *ChemPhysChem* **8**, 2464–2470 (2007).
- <sup>77</sup>W. R. Smith, S. Figueroa-Gerstenmaier, and M. Skvorova, "Molecular simulation for thermodynamic properties and process modeling of refrigerants," *Journal of Chemical & Engineering Data* **59**, 3258–3271 (2014).
- <sup>78</sup>D. H. Zaitsau, J. Neumann, A. Strate, *et al.*, "Isolating the role of hydrogen bonding in hydroxyl-functionalized ionic liquids by means of vaporization enthalpies, infrared spectroscopy and molecular dynamics simulations," *Physical Chemistry Chemical Physics* **21**, 20308–20314 (2019).
- <sup>79</sup>J. G. Harris, "Liquid-vapor interfaces of alkane oligomers: structure and thermodynamics from molecular dynamics simulations of chemically realistic models," *The Journal of Chemical Physics* **96**, 5498–5504 (1992).
- <sup>80</sup>J. Luo, C. Zhou, Q. Li, and L. Liu, "A unified approach for calculating free energies of liquid and defective crystals based on thermodynamic integration," *The Journal of Chemical Physics* **156** (2022).
- <sup>81</sup>M. Emamian, H. Azizpour, H. Moradi, K. Keynejad, H. Bahmanyar, and Z. Nasrollahi, "Performance of molecular dynamics simulation for predicting of solvation free energy of neutral solutes in methanol," *Chemical Product and Process Modeling* **17**, 489–497 (2022).
- <sup>82</sup>A. Z. Panagiotopoulos, "Direct determination of phase coexistence properties of fluids by monte carlo simulation in a new ensemble," *Molecular Physics* **61**, 813–826 (1987).
- <sup>83</sup>I. Nitzke, G. Guevara-Carrion, D. Saric, S. Homes, S. Stephan, R. Fingerhut, M. Bernreuther, H. Hasse, and J. Vrabec, "ms2: A molecular simulation tool for thermodynamic properties, release 5.0," *Computer Physics Communications* **310**, 109541 (2025).
- <sup>84</sup>G. E. Karniadakis, I. G. Kevrekidis, L. Lu, P. Perdikaris, S. Wang, and L. Yang, "Physics-informed machine learning," *Nature Reviews Physics* **3**, 422–440 (2021).
- <sup>85</sup>C. Meng, S. Griesemer, D. Cao, S. Seo, and Y. Liu, "When physics meets machine learning: a survey of physics-informed machine learning," *Machine Learning for Computational Science and Engineering* **1**, 20 (2025).
- <sup>86</sup>K. Kashinath, M. Mustafa, A. Albert, J.-L. Wu, C. Jiang, S. Esmailzadeh, K. Azizzadenesheli, R. Wang, A. Chattopadhyay, A. Singh, *et al.*, "Physics-informed machine learning: case studies for weather and climate modelling," *Philosophical Transactions of the Royal Society A: Mathematical, Physical and Engineering Sciences* **379** (2021).
- <sup>87</sup>M. Raissi, P. Perdikaris, and G. E. Karniadakis, "Physics-informed neural networks: A deep learning framework for solving forward and inverse problems involving nonlinear partial differential equations," *Journal of Computational physics* **378**, 686–707 (2019).
- <sup>88</sup>S. Zhu, L. Wang, C. Luo, *et al.*, "Physics-informed machine learning and its structural integrity applications: state of the art," *Philosophical Transactions of the Royal Society A: Mathematical, Physical and Engineering Sciences* **381**, 20220406 (2023).
- <sup>89</sup>G. C. Sosso and M. Bernasconi, "Harnessing machine learning potentials to understand the functional properties of phase-change materials," *Mrs Bulletin* **44**, 705–709 (2019).
- <sup>90</sup>J.-L. Wu, H. Xiao, and E. Paterson, "Physics-informed machine learning approach for augmenting turbulence models: A comprehensive framework," *Physical Review Fluids* **3**, 074602 (2018).
- <sup>91</sup>F. Jirasek, R. Bamler, and S. Mandt, "Hybridizing physical and data-driven prediction methods for physicochemical properties," *Chemical Communications* **56**, 12407–12410 (2020).
- <sup>92</sup>L. Prokhorenkova, G. Gusev, A. Vorobev, A. V. Dorogush, and A. Gulin, "Catboost: unbiased boosting with categorical features," *Advances in neural information processing systems* **31** (2018).
- <sup>93</sup>CAS, a division of the American Chemical Society, "CAS Common Chemistry," <https://commonchemistry.cas.org/>, accessed: Feb 18, 2026.

- <sup>94</sup>P. J. Linstrom and W. G. Mallard, "The nist chemistry webbook: A chemical data resource on the internet," *Journal of Chemical & Engineering Data* **46**, 1059–1063 (2001).
- <sup>95</sup>H. E. Pence and A. Williams, "Chemspider: an online chemical information resource," (2010).
- <sup>96</sup>D. S. Wishart, Y. D. Feunang, A. C. Guo, E. J. Lo, A. Marcu, J. R. Grant, T. Sajed, D. Johnson, C. Li, Z. Sayeeda, N. Assempour, I. Iynkkaran, Y. Liu, A. Maciejewski, N. Gale, A. Wilson, L. Chin, R. Cummings, D. Le, A. Pon, C. Knox, and M. Wilson, "DrugBank 6.0: the DrugBank Knowledgebase for 2024," *Nucleic Acids Research* **52**, D1265–D1275 (2024).
- <sup>97</sup>J. Wagner, M. Thompson, D. Dotson, A. L. East, P. K. Behara, T. Gokey, J. Horton, H. Jang, D. Cole, C. I. Bayly, D. L. Mobley, and J. Rodríguez-Guerra, "openforcefield/openff-forcefields: Version 2.0.0 "Sage"," (2021).
- <sup>98</sup>D. Van Der Spoel, E. Lindahl, B. Hess, G. Groenhof, A. E. Mark, and H. J. Berendsen, "Gromacs: fast, flexible, and free," *Journal of Computational Chemistry* **26**, 1701–1718 (2005).
- <sup>99</sup>C. Lu, C. Wu, D. Ghoreishi, W. Chen, L. Wang, W. Damm, G. A. Ross, M. K. Dahlgren, E. Russell, C. D. Von Bargen, *et al.*, "Opls4: improving force field accuracy on challenging regimes of chemical space," *Journal of chemical theory and computation* **17**, 4291–4300 (2021).
- <sup>100</sup>M. P. Allen and D. J. Tildesley, "Computer simulation of liquids," (2017).
- <sup>101</sup>G. Landrum *et al.*, "Rdkit documentation," Release **1**, 4 (2013).
- <sup>102</sup>J. Gasteiger and M. Marsili, "Iterative partial equalization of orbital electronegativity—a rapid access to atomic charges," *Tetrahedron* **36**, 3219–3228 (1980).
- <sup>103</sup>L. Martínez, R. Andrade, E. G. Birgin, and J. M. Martínez, "Packmol: A package for building initial configurations for molecular dynamics simulations," *Journal of computational chemistry* **30**, 2157–2164 (2009).
- <sup>104</sup>U. Essmann, L. Perera, M. L. Berkowitz, T. Darden, H. Lee, and L. G. Pedersen, "A smooth particle mesh ewald method," *The Journal of chemical physics* **103**, 8577–8593 (1995).
- <sup>105</sup>G. Bussi, D. Donadio, and M. Parrinello, "Canonical sampling through velocity rescaling," *The Journal of chemical physics* **126** (2007).
- <sup>106</sup>B. Hess, H. Bekker, H. J. Berendsen, and J. G. Fraaije, "Lincs: A linear constraint solver for molecular simulations," *Journal of computational chemistry* **18**, 1463–1472 (1997).
- <sup>107</sup>D. J. Evans and B. Holian, "The nose–hoover thermostat," *A)'=(A Is)* **1**, 18 (1985).
- <sup>108</sup>T. Akiba, S. Sano, T. Yanase, T. Ohta, and M. Koyama, "Optuna: A next-generation hyperparameter optimization framework," in *Proceedings of the 25th ACM SIGKDD international conference on knowledge discovery & data mining* (2019) pp. 2623–2631.
- <sup>109</sup>R. F. Woolson, "Wilcoxon signed-rank test," *Wiley encyclopedia of clinical trials*, 1–3 (2007).
- <sup>110</sup>P. W. Atkins, J. de Paula, and J. Keeler, *Atkins' Physical Chemistry*, 11th ed. (Oxford University Press, Oxford, 2018).
- <sup>111</sup>T. Dietterich, "Overfitting and undercomputing in machine learning," *ACM computing surveys (CSUR)* **27**, 326–327 (1995).
- <sup>112</sup>M. M. Bejani and M. Ghatee, "A systematic review on overfitting control in shallow and deep neural networks," *Artificial Intelligence Review* **54**, 6391–6438 (2021).
- <sup>113</sup>A. Adadi and M. Berrada, "Peeking inside the black-box: a survey on explainable artificial intelligence (xai)," *IEEE access* **6**, 52138–52160 (2018).
- <sup>114</sup>A. Lavecchia, "Explainable artificial intelligence in drug discovery: bridging predictive power and mechanistic insight," *Wiley Interdisciplinary Reviews: Computational Molecular Science* **15**, e70049 (2025).
- <sup>115</sup>C. Calc, "Joback Method Critical Properties Calculator [Web Application]," <https://toricalc.com/critical-properties/joback> (2026), retrieved 2026-01-20.
- <sup>116</sup>M. Hoffmann, T. Specht, N. Hayer, H. Hasse, and F. Jirasek, "Mlprop—an interactive web interface for thermophysical property prediction with machine learning," *Chemie Ingenieur Technik* **97**, 1052–1056 (2025).
- <sup>117</sup>A. Tropsha, "Best practices for qsar model development, validation, and exploitation," *Molecular informatics* **29**, 476–488 (2010).
- <sup>118</sup>A. Kubincová and D. L. Mobley, "Bridging between structure-based and data-driven affinity prediction," (2026).
- <sup>119</sup>M. Ahrenberg, M. Beck, C. Neise, O. Keßler, U. Kragl, S. P. Verevkin, and C. Schick, "Vapor pressure of ionic liquids at low temperatures from ac-chip-calorimetry," *Physical Chemistry Chemical Physics* **18**, 21381–21390 (2016).

# Thermodynamic Descriptors from Molecular Dynamics as Features for Extrapolable Property Prediction. (Supplementary Material)

Nuria H. Espejo<sup>1,2,+</sup>, Pablo Llombart<sup>1,+</sup>, Andres González de Castilla<sup>3</sup>, Jorge Ramirez<sup>4,\*</sup>, Jorge R. Espinosa<sup>1,5,6,7\*</sup>, Adiran Garaizar<sup>2,\*</sup>

[1] Department of Physical-Chemistry, Universidad Complutense de Madrid, Av. Complutense s/n, Madrid 28040, Spain

[2] Data Science, Bayer AG, Alfred-Nobel-Straße 50, 40789 Monheim am Rhein, Germany

[3] Bayer Crop Protection Innovation, Kaiser-Wilhelm-Alle 1, 51373 Leverkusen, Germany

[4] Department of Chemical Engineering, Universidad Politécnica de Madrid, C/ Jose Gutierrez Abascal 2, Madrid 28006, Spain

[5] Yusuf Hamied Department of Chemistry, University of Cambridge, Lensfield Road, Cambridge CB2 1EW, UK

[6] PhAsIca Biosciences S.L, Calle Velazquez, 27, 28001 Madrid, Spain

[7] Multidisciplinary Institute, Complutense University of Madrid, Paseo Juan XXIII, 1, Madrid 28040, Spain.

\* = To whom correspondence should be sent. email: jorge.ramirez@upm.es, jorgerene@ucm.es, adiran.garaizarsuarez@bayer.com

## SI. TANIMOTO SIMILARITY ANALYSIS METHODOLOGY

To quantify the structural novelty of the benchmark set relative to different training domains, we performed a Tanimoto similarity analysis using the RDKit toolkit. Morgan fingerprints (256-bit, radius 2) were generated for all molecules in our internal training set, the GRAPPA training set, and our external benchmark set. For each compound in the benchmark set, we calculated its maximum Tanimoto similarity to any molecule in a given training set (either our own or GRAPPA's). This score, ranging from 0 to 1, represents the compound's proximity to the most similar entry in the training domain. This process allowed us to stratify the benchmark set by structural similarity and directly assess how each model's predictive accuracy degrades as a function of increasing chemical novelty, thereby providing a rigorous measure of extrapolative performance.

## SII. SUPPLEMENTARY FIGURES

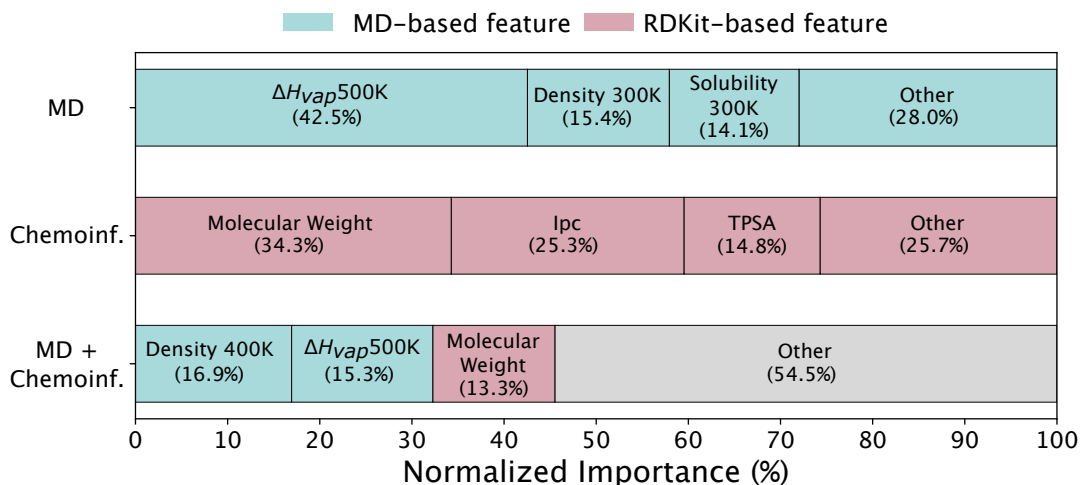


FIG. S1. Normalized feature importance (in %) for the OpenFF-based model architectures. The horizontal bars show the relative contribution of the most significant features. Blue segments represent MD-derived features red segments represent chemoinformatics descriptors, and gray represents the cumulative importance of either minor structural features. Top bar (MD-only, 3 features selected): Importance is concentrated in thermodynamic features like the heat of vaporization ( $\Delta H_{vap}$ ). Middle bar (Chemoinformatics-only, >1000 features used): Importance is led by molecular weight, followed by the information content of the characteristic polynomial (Ipc) and Topological Polar Surface Area (TPSA). Bottom bar (Hybrid, >1000 features used): A synergistic model where a thermodynamic features are complemented by key structural descriptors.

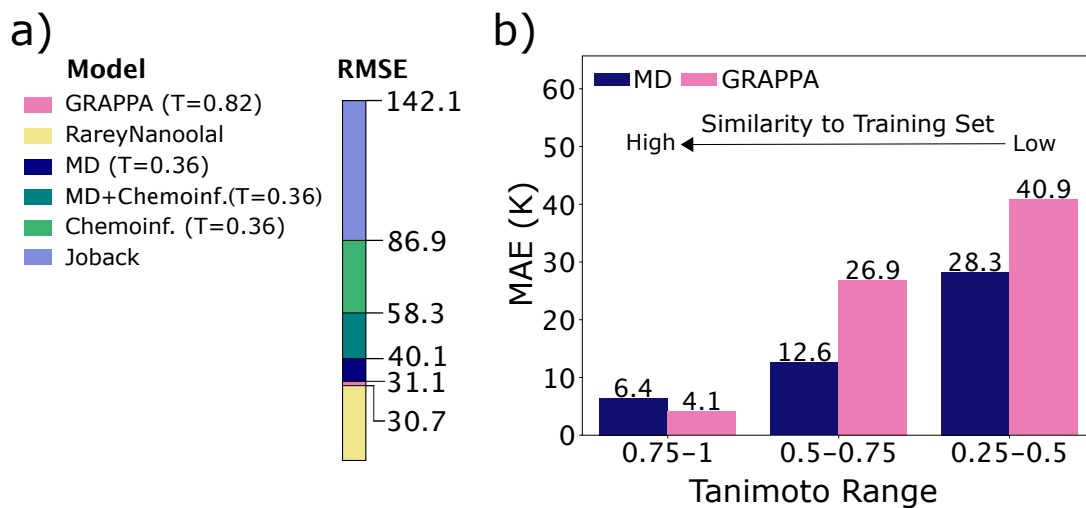


FIG. S2. Detailed performance analysis including the high-similarity regime. (a) Root Mean Square Error (RMSE) for the curated test set across various models: GRAPPA (pink), Rarey-Nanolal (yellow), MD-only (dark blue), hybrid MD+chemoinformatics (dark green), chemoinformatics-only (light green), and the Joback method (light blue). (b) MAE comparison between the MD-only model (dark blue) and GRAPPA (pink), stratified by Tanimoto similarity. This analysis includes the full similarity range up to 1.0, combining the moderate and high similarity compounds into a single bin (0.75-1.0).